Princeton Plasma Physics Laboratory

PPPL-4028

PPPL-4028

Exploiting a Transmission Grating Spectrometer

Ronald E. Bell

December 2004

Prepared for the U.S. Department of Energy under Contract DE-AC02-76CH03073.

PPPL Report Disclaimers

Full Legal Disclaimer

Trademark Disclaimer

PPPL Report Availability

This report is posted on the U.S. Department of Energy's Princeton Plasma Physics Laboratory Publications and Reports web site in Fiscal Year 2005. The home page for PPPL Reports and Publications is: http://www.pppl.gov/pub_report/

Office of Scientific and Technical Information (OSTI):

Available electronically at: http://www.osti.gov/bridge.

Available for a processing fee to U.S. Department of Energy and its contractors, in paper from:

U.S. Department of Energy
Office of Scientific and Technical Information
P.O. Box 62
Oak Ridge, TN 37831-0062

Telephone: (865) 576-8401

Fax: (865) 576-5728

E-mail: reports@adonis.osti.gov

National Technical Information Service (NTIS):

This report is available for sale to the general public from:

U.S. Department of Commerce
National Technical Information Service
5285 Port Royal Road
Springfield, VA 22161

Telephone: (800) 553-6847

Fax: (703) 605-6900

Email: orders@ntis.fedworld.gov

Online ordering: http://www.ntis.gov/ordering.htm

Exploiting a transmission grating spectrometer

Ronald E. Bell

Princeton Plasma Physics Laboratory, Princeton University, Princeton NJ, 08543-0451

The availability of compact transmission grating spectrometers now allows an attractive and economical alternative to the more familiar Czerny-Turner configuration for many high-temperature plasma applications. Higher throughput is obtained with short focal length refractive optics and stigmatic imaging. Many more spectra can be obtained with a single spectrometer since smaller, more densely packed optical input fibers can be used. Multiple input slits, along with a bandpass filter, can be used to maximize the number of spectra per detector, providing further economy. Curved slits can correct for the strong image curvature of the short focal length optics. Presented here are the governing grating equations for both standard and high-dispersion transmission gratings, defining dispersion, image curvature, and desired slit curvature, that can be used in the design of improved plasma diagnostics.

I. INTRODUCTION

Spectroscopy is an important tool of high temperature plasmas diagnostics. Impurity content, plasma temperature, and plasma flow are some of the quantities accessible using optical spectroscopy. The Czerny-Turner configuration[1] has long been the spectrometer of choice for these measurements, able to scan over a wide spectral range with a variety of dispersions. A plane grating, located between collimating and focussing mirrors, is rotated to vary wavelength. Off-axis imaging leads to a number of aberrations[2], including astigmatism and coma. A number of techniques have been used to mitigate these aberrations, e.g. coma can be corrected at a single wavelength, and astigmatism can be reduced with the use of toroidal mirrors. Most Czerny-Turner commercial spectrometers use a focal ratio of f/5-f/9.

Recent advances in commercializing volume phase holographic (VPH) gratings[3] have brought new compact spectrometers that offer many advantages over the popular Czerny-Turner configuration, including high throughput (f/1.8), stigmatic imaging and high grating efficiency. VPH gratings use a sinusoidally varying index of refraction in a dichromated gelatin medium to diffract light. The grating has a finite depth and Bragg diffraction controls the energy distribution of the diffracted light. The angle of the modulated index, and the thickness of the medium are adjusted to optimize the efficiency of the grating at a particular wavelength. Transmission grating spectrometers using this VPH technology are commercially available and are largely marketed for Raman spectroscopy under the name Holospec by Kaiser Optical Systems.[4, 5] In the Holospec spectrometer, a transmission grating is located between two commercial camera lenses at a fixed angle to maintain a 90° deviation. Commercial camera lenses insure superb imaging. Each grating is made for a particular wavelength range which remains fixed. A number of grating mounts are available to obtain a range of dispersions and bandwidths.

With the transmission grating spectrometer, coupling of fibers optics to the input of these spectrometers is simpler since the numerical aperture of the fiber optic closely matches that of the spectrometer, eliminating the need for inefficient matching optics. In a typical Czerny-Turner configuration, the ~f/2 fiber optic would have to be magnified ~2-5 times to match the ~f/5-f/9 spectrometer. With the on-axis stigmatic imaging and

camera lens optics, fibers can be closely stacked at the entrance slit without concern of crosstalk in the detector plane. The typical grating efficiency for VPH gratings is 80% for unpolarized light. Due to the Bragg condition for the gratings considered, only first order light is diffracted. The short focal length of the camera lenses (50-85 mm) produce strong spectral line curvature in the detector plane.

The transmission grating spectrometer has an overwhelming advantage over the Czerny-Turner spectrometer in throughput and imaging, but it lacks the ability for scanning. A fixed wavelength, however, is not a problem for many high temperature plasma diagnostic applications which monitor one or at most a few important emission lines or a fixed wavelength range. The spectral line curvature can easily be overcome with curved slits, as will be shown below. The low *f* number of transmission grating spectrometers offers the opportunity to significantly increase the number of detected photons, reducing the cost of a diagnostic system. The stigmatic imaging allows more spectra to be obtained with each detector, further improving economy.

The purpose of this paper is to present grating equations for a transmission grating spectrometer with emphasis on two grating configurations available for the Kaiser Holospec transmission grating spectrometers. These are intended to aid in the design of new diagnostics with improved performance and economy. A number of techniques and examples to fully exploit the advantages of this spectrometer are also presented.

II. GRATING EQUATIONS

The grating equation for the spectrometer shown in Fig. 1 is given by,

$$\lambda\nu = \cos\gamma\left[\sin\left(\theta_1 + \phi_1\right) + \sin\left(\theta_2 + \phi_2\right)\right], \qquad (1)$$

where λ is the wavelength, ν is the spatial frequency of the grating, γ is the vertical angle made by an off-axis ray, θ_1 is the angle of incidence at the optical axis, θ_2 is the angle of refraction at the central wavelength, ϕ_1 is the horizontal angular position of the entrance slit, and ϕ_2 is the horizontal angle in the image plane from the optical axis. Both θ_1 and θ_2 are constants as defined here. For the Kaiser Optical spectrometers represented in Fig. 1, there is an angular deviation of 90° between entrance slit and detector, so $\theta_1 + \theta_2 = 90°$. Angles are defined from the optical axis as follows, $\tan\phi_1 = x_1 / f_1$, $\tan\phi_2 = x_2 / f_2$, and

$\tan\gamma = y_1/f = y_2/f_2$. The horizontal distance x_1 is the position of the entrance slit from the optical axis, x_2 is the horizontal distance in the image plane, y_1 is the vertical position along the entrance slit, y_2 is the vertical position in the image plane, and f_1 and f_2 are the focal length of the collimating and focussing lenses, respectively. For a transmission grating centered at 5300 Å, $\theta_1 = 40°$. Typical values for f_1 are 85 mm.

The spatial frequency of the grating is defined by the central wavlength of the grating. On the optical axis, $\gamma = \phi_1 = \phi_2 = 0$. Here the chosen central wavelength specifies the required spatial frequency,

$$\nu = \frac{\sin\theta_1 + \sin\theta_2}{\lambda_0}, \qquad (2)$$

where λ_0 is the central wavelength. By differentiating Eq. (1) with respect to x_2, and using Eq. (2), the reciprocal linear dispersion is given by,

$$\frac{\partial\lambda}{\partial x_2} = \left(\frac{\lambda_0}{f_2}\right)\frac{\cos\gamma\cos(\theta_2+\phi_2)\cos^2\phi_2}{(\sin\theta_1+\sin\theta_2)}. \qquad (3)$$

The dispersion is fixed by the central wavelength and varies somewhat across the image plane. For a slit at the optical axis, the wavelength range spanned by a detector of width, w, can be approximated by,

$$\Delta\lambda \approx \lambda_0\frac{w}{f_2}\left(\frac{\cos\theta_2}{\sin\theta_1+\sin\theta_2}\right). \qquad (4)$$

Any spectral feature, such as an emission line, will have a strong curvature in the image plane due to the dependence of λ on γ in Eq. (1). Assuming small angles in the image plane, $\gamma << 1$ and $\Delta x_2 << f_2$, the deviation in horizontal position of a line of wavelength λ is given by the parabolic form,

$$\Delta x_2 = \left(\frac{\lambda}{\lambda_0}\right)\frac{(\sin\theta_1+\sin\theta_2)}{2f_2\cos(\theta_2+\phi_2)}y_2^2 . \qquad (5)$$

This can be approximated by a circle with radius,

$$R_{image} = \left(\frac{\lambda_0}{\lambda}\right)\frac{f_2\cos(\theta_2+\phi_2)}{(\sin\theta_1+\sin\theta_2)} . \qquad (6)$$

By curving the entrance slit, a straight image can be obtained at one wavelength using the radius,

$$R_{slit} = \left(\frac{\lambda_0}{\lambda}\right)\frac{f_1 \cos(\theta_1 + \phi_1)}{(\sin\theta_1 + \sin\theta_2)} \ . \qquad (7)$$

Note that since $\lambda \approx \lambda_0$, the slit curvature remains appropriate with gratings of differing central wavelengths. The optimal radius of curvature varies almost linearly with the distance of the entrance slit from the optical axis.

III. HIGH DISPERSION GRATING

It is not possible to increase dispersion at a given wavelength by simply increasing the spatial frequency of the grating, as can be seen from Eq. (2). A higher dispersion system using a transmission grating sandwiched between two right angle prisms does provides a higher dispersion option (see Fig. 2). This grating-prism combination is similar to those used for telecommunications.[5] Light is diffracted through 120°, and a silvered surface reflects back the diffracted light maintaing the 90° deviation. The reflected light is not refracted when it passes through the grating a second time, since, at that angle, the necessary Bragg condition is not met. The prisms are made of BK7 glass. The normal to the grating is tilted by 5° from the optical axis preventing back reflections.

The grating equation for this high dispersion grating is the same as in Eq. (1) above with the angles now defined in the glass medium. In this section, angles external to the prisms will be designated with a prime (′), and internal angles will be defined with respect to external angles. Assuming the index of refraction of air equals 1, the angles across the air-glass interface are defined using Snell's law: $n\sin\varepsilon_0 = \sin\varepsilon'$, $n\sin\varepsilon_1 = \sin(\varepsilon' - \phi_1')$, $n\sin\varepsilon_2 = \sin(\varepsilon' - \phi_2')$, and $n\sin\gamma = \sin\gamma'$, where $\varepsilon' = 5°$ is the angle between the optical axis and the prism surface normal, and $n = n(\lambda)$ is the index of refraction of BK7 glass. As before, $\tan\phi_1' = x_1/f_1$, $\tan\phi_2' = x_2/f_2$, and $\tan\gamma' = y_1/f_1 = y_2/f_2$. In order to maintain the same form in the grating equations, *the direction of x_1 is opposite to that defined in the previous section* due to the reflection of the diffracted light by the silvered surface. The behavior in the image plane is consistent for both grating types, with wavelength increasing to the right if facing the detector from the grating, see Figs. 1, 2. The direction of curvature of the entrance slit to compensate

for spectral line curvature will be opposite for the high dispersion case, but will always curve toward increasing x_1.

With a little geometry, it can be shown that the internal angles in Eq. (1) are given by: $\theta_1 = \theta_p - \varepsilon_0$, $\phi_1 = \varepsilon_0 - \varepsilon_1$, $\phi_2 = \varepsilon_0 - \varepsilon_2$, and $\theta_2 = 120^\circ - \theta_1$, where the prism angle $\theta_p = 63°17'30"$. This also implies that $\theta_1 + \phi_1 = \theta_p - \varepsilon_1$ and $\theta_2 + \phi_2 = \theta_p - \varepsilon_2$, and $\theta_1 \approx \theta_2 \approx 60°$. The spatial frequency of the high dispersion grating is given by Eq. (2), using the above definitions for the internal angles. The reciprocal linear dispersion is computed as,

$$\frac{\partial \lambda}{\partial x_2} = \frac{\partial \lambda}{\partial \phi_2}\frac{\partial \phi_2}{\partial \varepsilon_2}\frac{\partial \varepsilon_2}{\partial \phi_2'}\frac{\partial \phi_2'}{\partial x_2}\ , \qquad (8)$$

which will take the form,

$$\frac{\partial \lambda}{\partial x_2} = \frac{\lambda_0}{n f_2}\frac{\cos\gamma\cos(\theta_2+\phi_2)\cos^2\phi_2'\cos(\varepsilon'-\phi_1)}{(\sin\theta_1+\sin\theta_2)\cos\varepsilon_2}. \qquad (9)$$

The covered wavelength range can be estimated by multiplying the central dispersion by the detector width. Given $\theta_1 \approx \theta_2 \approx 60°$, the estimated range for visible wavelengths is,

$$\Delta\lambda \approx \frac{w\lambda_0}{2n(\lambda_0)f_2\tan 60^\circ} \approx 0.190\frac{w\lambda_0}{f_2}. \qquad (10)$$

The spectral line curvature can be approximated with a circle of radius,

$$R_{image} = \left(\frac{\lambda_0}{\lambda}\right)\left(\frac{n f_2\cos(\theta_2+\phi_2)}{\sin\theta_1+\sin\theta_2}\right)\left(\frac{\cos(\varepsilon'-\phi_2')}{\cos\varepsilon_2}\right). \qquad (11)$$

To compensate for the spectral line curvature, the radius of curvature of the entrance slit required is given by,

$$R_{slit} = \left(\frac{\lambda_0}{\lambda}\right)\left(\frac{n f_1\cos(\theta_1+\phi_1)}{\sin\theta_1+\sin\theta_2}\right)\left(\frac{\cos(\varepsilon'-\phi_1')}{\cos\varepsilon_1}\right). \qquad (12)$$

The first term, λ/λ_0, and, last term, the ratio of cosines, in Eq. (11) and Eq. (12) are quite close to unity. A rough estimate, assuming a centered slit, and a typical index of refraction, gives $R_{slit} \approx 0.436 f_1$.

The index of refraction for BK7 varies with wavelength and can be conveniently calculated from the Sellmeier dispersion formula,

$$n(\lambda) = \sqrt{1 + \frac{B_1\lambda^2}{(\lambda^2 - C_1)} + \frac{B_2\lambda^2}{(\lambda^2 - C_2)} + \frac{B_3\lambda^2}{(\lambda^2 - C_3)}} \quad , \qquad (13)$$

where λ is in units of microns and for BK7 glass: B_1=1.03961212, B_2=0.231792344, B_3=1.01046945, C_1=0.00600069867, C_2=200.179144, C_3=103.560653.[6]

IV. OPTIMIZING

There are a number of enchancements to these spectrometers that allow a full exploitation of their potential. The stimagtic imaging allows individual fibers to be stacked close together, increasing the number of spectra that can be obtained with a single detector. If the desired wavelength range needed for a diagnostic application is less that the values indicated in Eq. (4) or Eq. (10), then multiple entrance slits can be distributed horizontally. A bandpass interference filter customized to the wavelength of interest can then be mounted on a standard camera filter and attached to the collimating lens.[7] When using a 2D detector, such as a CCD, it is often desirable to bin pixels vertically to improve signal to noise or to read out the CCD more quickly. The spectral line curvature will degrade the otherwise narrow instrumental function of these spectrometers, especially at the vertical extremes. Curving the entrance slit, to straighten the image will eliminate this effect. Higher throughput allows shorter integrations times which may approach vertical transfer times when using CCD detectors. With multiple spectra there is a need to block the light falling on the CCD during this transfer time. A mechanical chopper sychronized to the CCD camera readout has been used to avoid this difficulty.[7,8]

Another technique to improve the light collection capabilities of these spectrometers is to choose a faster, shorter focal length output lens. For example, with an input lens of 85 mm, f/1.8 coupled to an output lens of 58 mm, f/1.2 the étendue is preserved and almost 50% more light can be collected, since the image of the detector appears larger and more fibers can be stacked in the entrance slit. This decreases the cost of a system, and is appropriate if the corresponding reduction in dispersion is tolerable.

Although all of the equations presented above assume that the entrance slit and detector are mounted at distances of f_1 and f_2, respectively, in practice it is slightly different. The Holospec spectrometers typically set the focus of input lens at values less

than infinity to allow a range of adjustment of the output lens to accomodate a mounted detector. On the National Spherical Torus Experiment (NSTX), the spectrometer and detector are mounted on commercially available translation and rotation stages to provide a 6–axis adjustable mount, which faciliates alignment of the CCD to the spectrometer.[8] Both lenses are then set at infinity and focus is achieved with the translation stage.

The transmission grating spectrometers described here have already been put to use in a number of high-temperature plasma diagnostics applications. These instruments have been used on the Tokamak Fusion Test Reactor to measure poloidal plasma flow[7], on the Current Drive Experiment Upgrade to measure electron temperature with Thomson scattering[9], on NSTX for charge exchange recombination spectroscopy, and for measurements of C III velocity[8], temperature and radial electric field at the plasma edge. A broad band grating has been used for edge electron temperature measurements using helium line ratios.[10] These spectrometers are also planned for use on JET for charge exchange spectroscopy and helium ash measurements.[11]

ACKNOWLEDGMENTS

This work was supported by DOE Contract No. DE-AC02-76-CH0307

---

[1] M. Czerny and A. F. Turner, Z. Phys. 61 , 792-797 (1930).
[2] See, e.g., references contained in: K. M. Rosfjord, R. A. Villalaz, T. K. Gaylord, Applied Optics, 39, 568 (2000).
[3] S. C. Barden, J. A. Arns, W. S. Colburn, Proc. SPIE, 3355, 866 (1998).
[4] H. Owen, D. E. Battey, M. J. Pelletier, J. B. Slater, Proc. SPIE 2406, 260 (1995).
[5] Kaiser Optical Systems, Inc., Ann Arbor, Michigan, http://www.kosi.com
[6] Schott Optical Glass Catalog, 2003, Schott Glas, Mainz, Germany, *http://www.schott.com*
[7] R. E. Bell, L. E. Dude, B. Grek, D. W. Johnson, R. W. Pallidino, Rev. Sci. Instrum, **70**, 821-826 (1999).
[8] T. M. Biewer, R. E. Bell, R. Feder, *et al.*, Rev. Sci. Instrum, **75**, 650-654 (2004).
[9] T. Munsat, B. LeBlanc, Rev. Sci. Instrum. **70**, 775-758 (1999).
[10] C. S. Pitcher, B. LaBombard, B. Lipshultz, J. L. Terry, R. E. Bell, S. J. Zweben, *Bulletin of the American Physical Society*, **45**, 319 (2000).
[11] D. L. Hillis, D. T. Fehling, R. E. Bell, D. W. Johnson, K-D Zastrow, A. Meigs, C. Negus, C. Giroud, M. Stamp, this conference.

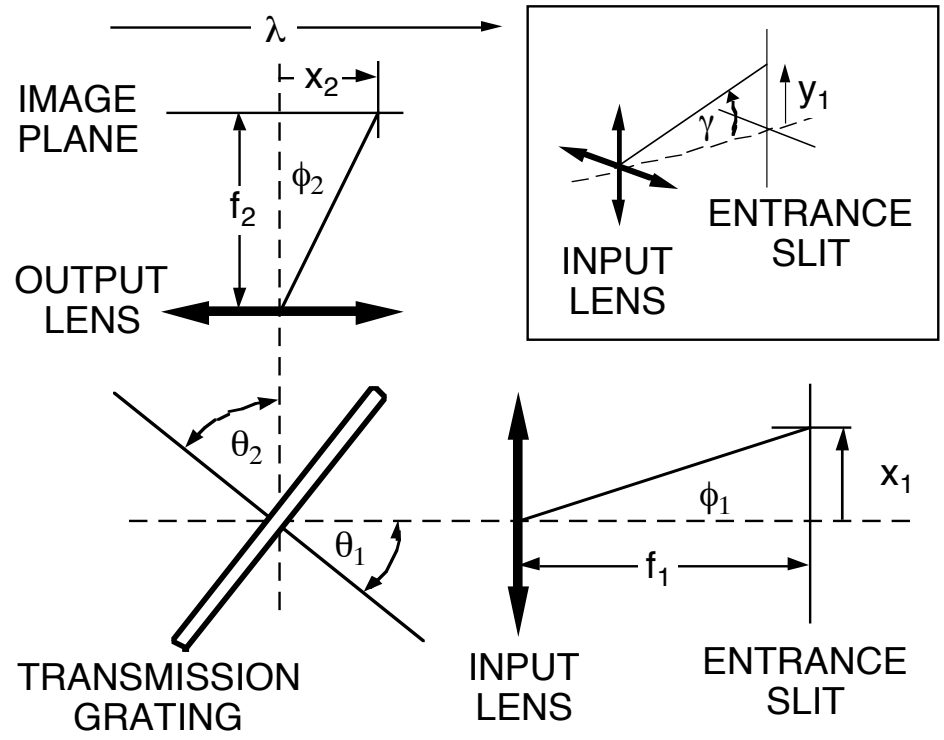

Fig. 1 Schematic of transmission grating spectrometer.

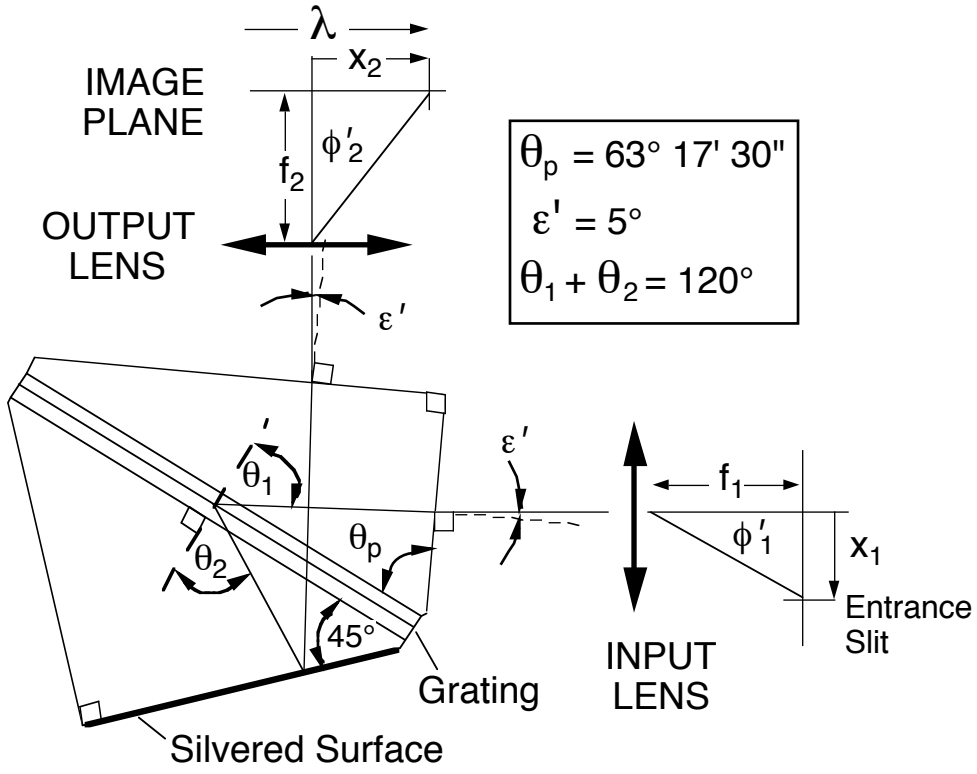

Fig. 2 Schematic of high disperion spectrometer with prism grating combination. Note that the direction of x_1 is defined to be opposite to that used in Fig. 1.

External Distribution

Plasma Research Laboratory, Australian National University, Australia

Professor I.R. Jones, Flinders University, Australia

Professor João Canalle, Instituto de Fisica DEQ/IF - UERJ, Brazil

Mr. Gerson O. Ludwig, Instituto Nacional de Pesquisas, Brazil

Dr. P.H. Sakanaka, Instituto Fisica, Brazil

The Librarian, Culham Laboratory, England

Mrs. S.A. Hutchinson, JET Library, England

Professor M.N. Bussac, Ecole Polytechnique, France

Librarian, Max-Planck-Institut für Plasmaphysik, Germany

Jolan Moldvai, Reports Library, Hungarian Academy of Sciences, Central Research Institute for Physics, Hungary

Dr. P. Kaw, Institute for Plasma Research, India

Ms. P.J. Pathak, Librarian, Institute for Plasma Research, India

Ms. Clelia De Palo, Associazione EURATOM-ENEA, Italy

Dr. G. Grosso, Instituto di Fisica del Plasma, Italy

Librarian, Naka Fusion Research Establishment, JAERI, Japan

Library, Laboratory for Complex Energy Processes, Institute for Advanced Study, Kyoto University, Japan

Research Information Center, National Institute for Fusion Science, Japan

Dr. O. Mitarai, Kyushu Tokai University, Japan

Dr. Jiangang Li, Institute of Plasma Physics, Chinese Academy of Sciences, People's Republic of China

Professor Yuping Huo, School of Physical Science and Technology, People's Republic of China

Library, Academia Sinica, Institute of Plasma Physics, People's Republic of China

Librarian, Institute of Physics, Chinese Academy of Sciences, People's Republic of China

Dr. S. Mirnov, TRINITI, Troitsk, Russian Federation, Russia

Dr. V.S. Strelkov, Kurchatov Institute, Russian Federation, Russia

Professor Peter Lukac, Katedra Fyziky Plazmy MFF UK, Mlynska dolina F-2, Komenskeho Univerzita, SK-842 15 Bratislava, Slovakia

Dr. G.S. Lee, Korea Basic Science Institute, South Korea

Institute for Plasma Research, University of Maryland, USA

Librarian, Fusion Energy Division, Oak Ridge National Laboratory, USA

Librarian, Institute of Fusion Studies, University of Texas, USA

Librarian, Magnetic Fusion Program, Lawrence Livermore National Laboratory, USA

Library, General Atomics, USA

Plasma Physics Group, Fusion Energy Research Program, University of California at San Diego, USA

Plasma Physics Library, Columbia University, USA

Alkesh Punjabi, Center for Fusion Research and Training, Hampton University, USA

Dr. W.M. Stacey, Fusion Research Center, Georgia Institute of Technology, USA

Dr. John Willis, U.S. Department of Energy, Office of Fusion Energy Sciences, USA

Mr. Paul H. Wright, Indianapolis, Indiana, USA

The Princeton Plasma Physics Laboratory is operated
by Princeton University under contract
with the U.S. Department of Energy.

Information Services
Princeton Plasma Physics Laboratory
P.O. Box 451
Princeton, NJ 08543

Phone: 609-243-2750
Fax: 609-243-2751
e-mail: pppl_info@pppl.gov
Internet Address: http://www.pppl.gov